PHYSICAL REVIEW A **87**, 030501(R) (2013)

g-factor measurement of hydrogenlike $^{28}Si^{13+}$ as a challenge to QED calculations

S. Sturm,[1,2] A. Wagner,[1] M. Kretzschmar,[2] W. Quint,[3] G. Werth,[2] and K. Blaum[1]
[1]*Max-Planck-Institut für Kernphysik, Saupfercheckweg 1, 69117 Heidelberg, Germany*
[2]*Institut für Physik, Johannes Gutenberg-Universität, 55099 Mainz, Germany*
[3]*GSI Helmholtzzentrum für Schwerionenforschung GmbH, Planckstraße 1, 64291 Darmstadt, Germany*
(Received 30 May 2012; published 8 March 2013)

Using a phase-detection method to determine the cyclotron frequency of a single trapped ion in a Penning trap allowed us to perform a measurement of the g factor of the bound electron in hydrogenlike $^{28}Si^{13+}$ with a statistical uncertainty of 4×10^{-11}. Furthermore, we reevaluated the image-charge shift as the main source of uncertainty. Our result challenges bound-state quantum-electrodynamical calculations by probing two-loop contributions of order $(Z\alpha)^6$ and paves the way towards a more precise determination of fundamental constants as the electron mass.

DOI: 10.1103/PhysRevA.87.030501 PACS number(s): 31.30.js, 06.20.Jr, 12.20.Fv, 37.10.Ty

Measurements of the g factor of the electron bound in hydrogenlike ions represent the most stringent test of bound-state quantum-electrodynamic (BS-QED) calculations. In the past, experiments have been performed on $^{12}C^{5+}$ [1], $^{16}O^{7+}$ [2], and $^{28}Si^{13+}$ [3] where the spin precession frequency of a single ion confined in a Penning trap with a superimposed strong homogeneous magnetic field has been determined with fractional uncertainties of 5×10^{-10}, 7×10^{-10}, and 5×10^{-10}, respectively. A remarkable agreement to theory at the level of 4×10^{-10} has been found, which made it possible to probe QED contributions up to the two-loop level of the order of $(Z\alpha)^4$ [3]. The precision of these experiments was limited mainly by statistics and in [1,2] by the ion's temperature of several 10 K, causing line broadening and shifts. In order to become sensitive to even higher order BS-QED contributions, whose estimated relative size for $^{28}Si^{13+}$ is 17×10^{-10}, we are attempting to reduce the experimental uncertainty. To this end we have developed a technique to determine the phase of the cyclotron oscillation of the single ion [4]. The method allows measuring the ion's oscillation frequencies, as required for calibration of the magnetic field strength, two orders of magnitude faster and more precise than direct frequency determinations. This enables higher data rates and reduced uncertainties from trap parameter fluctuations. Moreover, the ion is kept at low temperature during the measurement, which reduces limitations from residual magnetic field inhomogeneities. As a result we reduced the statistical uncertainty of our previous experiment on $^{28}Si^{13+}$ by one order of magnitude. This will lead to a breakthrough in measurements of fundamental properties. We also reexamined the largest systematical shift of the ion oscillation frequencies caused by induced image charges and reduced its contribution to the error budget.

In this Rapid Communication we report on a measurement of the g factor of the bound electron in $^{28}Si^{13+}$ with a measurement uncertainty of 4×10^{-11}, which will make it possible to probe BS-QED calculations to the order $(Z\alpha)^6$, whose calculation represents a challenge for theory (see Fig. 1). For our experiment we use the same $^{28}Si^{13+}$ ion as in the experiment described in Refs. [3,4]. It was stored for 7 months in a cylindrical Penning trap in thermal contact to a liquid helium bath, with a superimposed magnetic field of $B \simeq 3.76$ T, at an estimated rest-gas pressure of less than 10^{-16} mbar. The trap has three different potential minima for ion storage. After creation in the first minimum ("creation trap"), cleaning from unwanted simultaneously trapped ions, and reduction of the ion number to a single one, we measured the three motional frequencies of a particle in a second minimum ("precision trap"). For the operating conditions in the precision trap the magnetron oscillation frequency amounts to $\nu_- \simeq 9$ kHz, the axial oscillation to $\nu_z \simeq 710$ kHz, and the modified cyclotron oscillation to $\nu_+ \simeq 27$ MHz. The experimental setup is described in detail in Refs. [3,6]. From the measurement of the three eigenfrequencies the cyclotron frequency ν_c of the ion can be determined using the Brown-Gabrielse invariance theorem [7]:

$$\nu_c^2 = \nu_+^2 + \nu_z^2 + \nu_-^2. \tag{1}$$

The axial motion is the only one which can be detected directly in our experiment by induced image currents in the trap's end-cap electrodes. These are picked up by a superconducting tank circuit with a quality factor of $Q = 3100$. The modified cyclotron oscillation and the magnetron oscillation are coupled to the axial motion by a radio-frequency field at the respective motional sidebands. Crucial for achieving high precision is that the measurements are performed as fast as possible in order to reduce the influence of temporal variations of the magnetic field on the precision of the frequency determination. At the same time the oscillation amplitudes, especially the critical cyclotron radius, should be kept as small as possible to reduce limitations by residual magnetic-field inhomogeneities and relativistic mass increase.

To this end we employed a phase measurement for the modified cyclotron oscillation of the coherently excited ion [3]. Initially, the ion is resistively cooled to the temperature of the environment. Excitation of its modified cyclotron oscillation is performed by a dipole field with well-defined phase. Then the phase of the cyclotron oscillation evolves freely for a given time. During this period, the high-quality tank circuit used to detect the axial motion is decoupled from the ion, so that none of the eigenmotions is disturbed by image-current interaction. Finally, the axial and cyclotron modes are coupled by a radio-frequency field at their sum frequency, which causes a parametric amplification of the cyclotron motion. During this

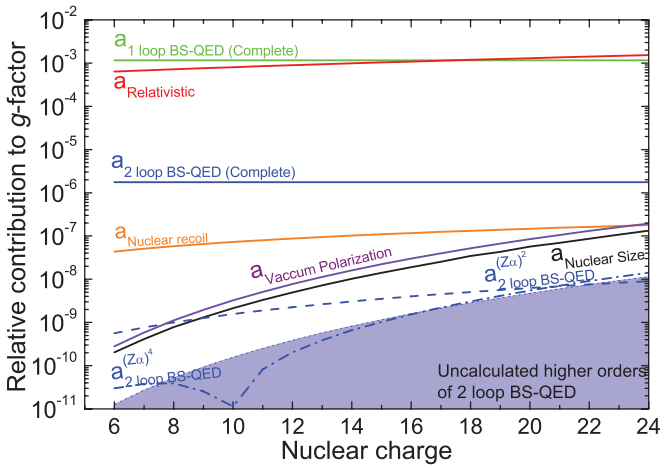

FIG. 1. (Color online) Contributions a to the magnetic moment anomaly $(g-2)/2$ of the bound electron, arising from bound-state QED and corrections due to the finite size and mass of the nucleus, for a range of nuclear charges [5].

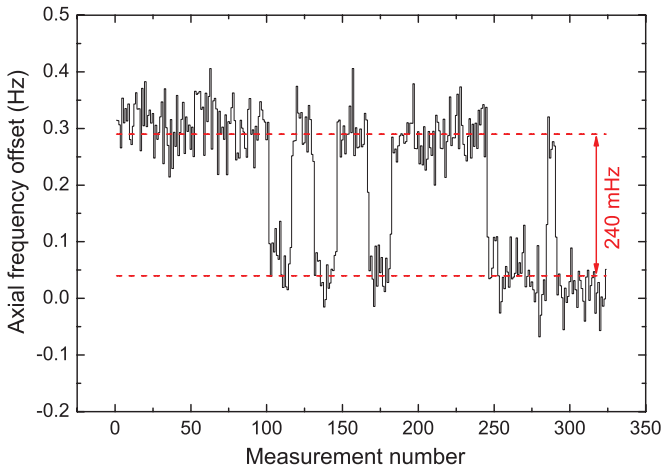

FIG. 2. (Color online) Recorded induced spin flips of the bound electron, manifested as a jump in the axial oscillation frequency of 412 kHz.

process, the cyclotron phase is imprinted onto the axial motion, which is being detected. The modified cyclotron frequency ν_+ can be reconstructed by measuring the phase as a function of the measurement time.

Simultaneously with the determination of the motional frequencies, microwaves of (nominally) 105 GHz are introduced into the apparatus to probe the spin transition of the bound electron. A successful spin flip is detected in a third potential minimum ("analysis trap") to which the ion is shifted after the microwave irradiation. Here, the magnetic field of the Penning trap is made on purpose inhomogeneous by a nickel ring electrode. The inhomogeneous field imposes a force on the electron's magnetic moment, which shifts the ion's axial oscillation frequency. When we make a series expansion of our magnetic field, $B = B_0 + B_2 z^2 + \cdots$, the second-order term B_2 amounts for our geometry to 10 $\frac{\mathrm{mT}}{\mathrm{mm}^2}$. This leads to a frequency shift of ± 120 mHz for the two spin orientations at an oscillation frequency of 412 kHz. A spin flip is then monitored by a jump in the axial oscillation frequency of 240 mHz. This has to be compared with a measured mean noise amplitude of the axial frequency of 21 mHz after averaging for 8 s, indicating that a spin flip can be detected with nearly 100% fidelity (see Fig. 2). Figure 3 shows the number of successful spin flips as a function of the microwave frequency ν_L. We plot the ratio $\Gamma \equiv \frac{\nu_{\mathrm{MW}}}{\nu_c}$, which makes the individual events independent of magnetic-field fluctuations to first order. The frequency ratio $\frac{\nu_L}{\nu_c}$ can be extracted from the data with a Gaussian fit using the maximum-likelihood method. Altogether, eight resonances similar to Fig. 3 were recorded for different cyclotron excitation energies. Although the excitation energy is typically small, at our level of precision, relativistic shifts become significant. With $\gamma = 1/\sqrt{1 - v^2/c^2}$ the cyclotron and Larmor precession frequency ν_c and ν_L write as $\nu_c = \frac{1}{2\pi}\frac{qB}{\gamma m}$ and $\nu_L = \frac{g}{4\pi}\frac{qB}{m} + (1-\gamma)\,\nu_c$, respectively. The term $(1-\gamma)\nu_c$ is the Thomas precession frequency, which is suppressed by a factor of ν_c/ν_L compared to the free electron case. We obtain

$$\delta\Gamma(E_+) \simeq \Gamma \frac{E_+}{m\,c^2}. \tag{2}$$

When we excite the cyclotron motion to a higher cyclotron energy E_+, calibrated through the resulting axial frequency shift in the magnetic bottle, we observe a linear increase of the Γ_0' value, as expected (Fig. 4). The frequency ratio for zero cyclotron energy is obtained by extrapolating the individual resonance centroids, yielding

$$\Gamma_0' \equiv \frac{\nu_L}{\nu_c} = 3912.866\,067\,49(13),$$

with a purely statistical fractional uncertainty of 4×10^{-11}. This is almost an order of magnitude more precise than reported in our previous g–factor determination of $^{28}\mathrm{Si}^{13+}$ [3].

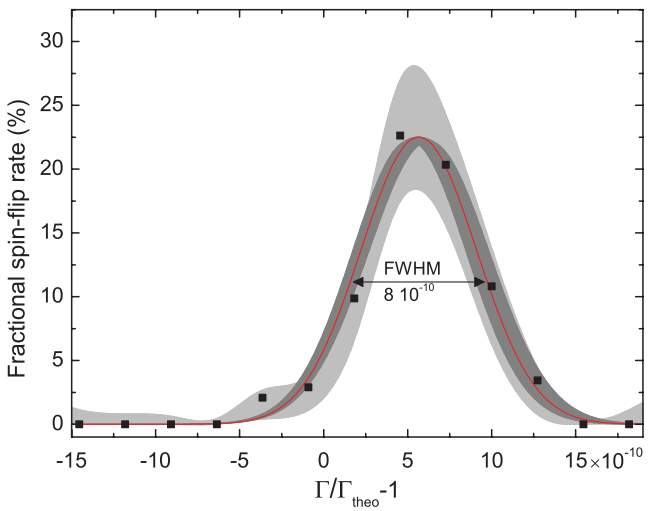

FIG. 3. (Color online) One of the eight recorded resonances. The light gray area represents the 1σ prediction band for the measurements, while the dark gray region displays the confidence band of the maximum-likelihood fit with respect to the centroid parameter.

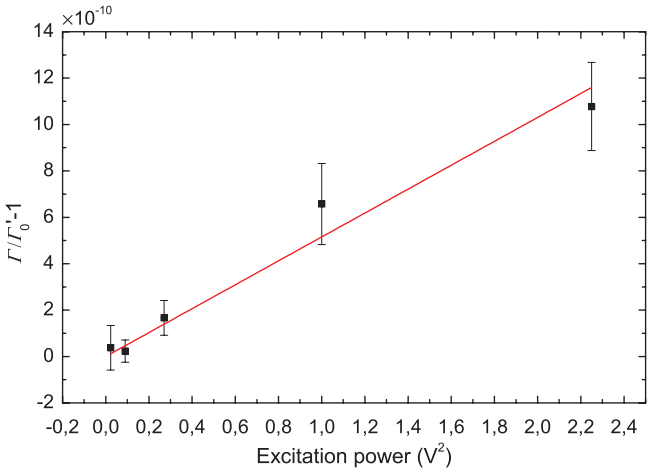

FIG. 4. (Color online) Individual uncorrected Γ values, determined from the centroids of the eight recorded resonances. Centroids with identical excitation energy have been contracted for clarity.

The value Γ_0' still has to be corrected for a number of systematic shifts from various sources. The dominant correction to the measured value arises from the charge distribution induced by the oscillating ion on the inner surface of the trap electrodes, a manifestation of so-called image charges. The charge distribution changes the trapping potential and thus shifts the value of the cyclotron frequency as determined via the invariance theorem. This effect has been studied by Van Dyck Jr. *et al.* [8] for a spherical trap geometry and by Porto [9] for cylindrical geometries. In order to account for the improved statistical precision of this measurement, we have reanalyzed the problem and refined the calculations in order to estimate the effect of specific construction details of our trap such as slits separating the various electrodes or the slit dividing one of the correction electrodes. In our experiment the ions stay within a distance of less than 200 μm from the trap center, monitored by the well-known magnetic field shape in the analysis trap. Therefore, it is justified to treat the additional potential energy term in the harmonic approximation. Assuming perfect alignment of the trap and the magnetic field and with an appropriate choice of the x and y axes the harmonic part of the image potential is given as a diagonal quadratic form,

$$U_{\rm im}(x,y,z) = -\frac{m}{2}(\Delta_x x^2 + \Delta_y y^2 + \Delta_z z^2), \tag{3}$$

where the parameters Δ_i have to be determined from the distribution of image charges on the electrodes. In this approximation the image force acting on the ion is

$$\vec{F}_{\rm im} = -\vec{\nabla} U_{\rm im} = m(\Delta_x x + \Delta_y y + \Delta_z z). \tag{4}$$

By Newton's third law the force on the ion must be oppositely equal to the sum of forces acting on the induced charges on the inner trap surfaces. This charge distribution and the forces acting on it can be calculated by well-known methods using Green's functions with Dirichlet boundary conditions on the inner trap surface [10,11]. Denoting the eigenfrequencies of the perturbed Hamiltonian $H = H_0 + U_{\rm im}(x,y,z)$ by $\bar{\nu}_+$, $\bar{\nu}_-$, and $\bar{\nu}_z$ one can show that the cyclotron frequency shift caused

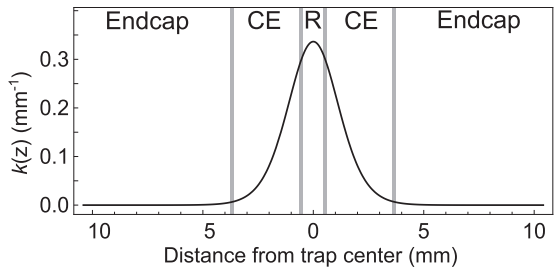

FIG. 5. Calculated image charge density $\kappa(z)$. The gray areas indicate the position of the radial insulating slits between the individual electrodes, where no image charge can be located. *CE* and *R* denote the correction electrodes and the ring electrode, respectively.

by the image potential

$$\delta\bar{\nu}_c = \nu_c - \bar{\nu}_c = \nu_c - \sqrt{\bar{\nu}_+^2 + \bar{\nu}_-^2 + \bar{\nu}_z^2}, \tag{5}$$

is determined by the parameters Δ_i,

$$\frac{\delta\bar{\nu}_c}{\nu_c} = \frac{\nu_c^2 - \bar{\nu}_c{}^2}{\nu_c(\nu_c + \bar{\nu}_c)} \simeq \frac{\Delta_x + \Delta_y + \Delta_z}{8\pi^2\nu_c^2}. \tag{6}$$

With $c_i = 4\pi\epsilon_0 m\, a^3\, \Delta_i/q^2 (i = x,y,z)$, where $a = 3.5$ mm is the cylinder radius, this relation becomes

$$\frac{\delta\bar{\nu}_c}{\nu_c} = \frac{m}{8\pi\epsilon_0 a^3 B_0^2}(c_x + c_y + c_z). \tag{7}$$

For a spherical trap $c_x = c_y = c_z = 1$ [8]. More generally we write c_i as an integral over the trap surface. For our trap geometry using a stack of cylinders we obtain an axial distribution of image charges $\kappa_i(z)$, such that $c_i = \int_{-L/2}^{L/2} dz \kappa_i(z)$. L is the length of the precision trap from end cap to end cap; in our case $L = 20.82$ mm. We can identify the contributions of the various electrodes including the insulating radial slits between them. The function $\kappa_i(z)$ is plotted in Fig. 5, with vertical areas indicating the positions of the radial slits.

To obtain an estimate of the frequency shift $\delta\bar{\nu}_c$ we integrate $\kappa_i(z)$ over the inner trap surface. For an upper limit the integration is extended over the full length L of the cylinder, including the areas corresponding to the slits. We obtain $c_x = c_y = 1.002\,725$ and $c_z \approx 0$. For a lower limit we repeat the calculation, but omit the areas corresponding to the slits, obtaining $c_x = 0.908\,426$, $c_y = 0.916\,145$, and $c_z \approx 0$. The inequality of c_x and c_y is caused by slits in the axial direction, separating two segments of one correction electrode that is required for the application of a radio-frequency field in the radial plane. A fraction of the charges which were originally in the area of the slits will arrange along the edges of the slit, such that the size of the frequency shift will amount to a value between the two calculated extremes. We take the average of the coefficients c_i from the two approaches to calculate the shift of the cyclotron frequency and arrive at

$$\frac{\delta\bar{\nu}_c}{\nu_c} = 1.92\frac{m}{8\pi\epsilon_0 a^3 B_0^2}, \tag{8}$$

quoting the difference of the two cases for c_i as uncertainty. For $^{28}Si^{13+}$ the correction amounts to $\delta\bar{\nu}_c/\nu_c = 6.59 \pm 0.33 \times 10^{-10}$.

Beyond that, a large variety of sources for systematic shifts have been considered. However, most of these are negligible

TABLE I. Dominant sources of systematic shifts, given in parts per trillion (ppt). For the energy-dependent effects, typical values for the lowest excitation are quoted.

Contribution	Relative shift of ν_c in ppt	Relative shift of Γ in ppt	Uncertainty of correction in ppt
Image charges	−659	+659	33
Magnetic inhomogeneity	<20	$\ll$10	$\ll$10
Dip lineshape	<4	<4	<4
Electrostatic anharmonicity	<0.1	<0.1	<0.1
Frequency pulling	<10	<10	<10

due to recent improvements of the cryogenic electronics and the detection method. By using negative electronic feedback cooling, a temperature of the tank circuit and consequently the axial motion of the ion below 1 K can be achieved [6,12]. This strongly relaxes the requirements on the harmonicity of the electrostatic trapping potential and the homogeneity of the magnetic field. During the phase sensitive cyclotron frequency detection, the cyclotron mode is completely decoupled from the detector, removing frequency pulling effects. Furthermore, since now the cyclotron motion is detected directly rather than as an offset to the axial frequency [3], the requirements on the accuracy of the axial frequency measurement are also relaxed. This removes the uncertainty due to the parameters of the fit function, which was among the largest contributions in previous measurements. In Table I the dominant systematic contributions are compiled.

With all corrections applied, we arrive at a value of

$$\Gamma_0 = 3912.866\,064\,99(13)(13). \tag{9}$$

The g factor is finally determined from

$$g = 2\frac{q}{e}\frac{m_e}{M}\frac{\nu_L}{\nu_c} = 2\frac{q}{e}\frac{m_e}{M}\Gamma_0, \tag{10}$$

where q is the ion's charge state, M its mass, and m_e the electron mass. Using $m_e = 5.485\,799\,094\,6(22) \times 10^{-4}$ u from the 2010 CODATA compilation of fundamental constants [13] and $M(^{28}\mathrm{Si}^{13+}) = 27.969\,800\,594\,9(7)$ u, from a measurement of the ^{28}Si mass by Redshaw *et al.* [14], corrected by the mass of the missing electrons and their binding energies [15], we can finally deduce the g factor as

$$g = 1.995\,348\,959\,10(7)(7)(80). \tag{11}$$

The first error represents the statistical uncertainty of the fit, the second one the systematic uncertainty, mainly due to the image charge shift. The third error is given by the current uncertainty of the electron mass. This value is in agreement with both the theoretical result $g_{\mathrm{th}} = 1.995\,348\,958\,0(17)$ and our previously published value $g_{\mathrm{ex}} = 1.995\,348\,958\,7(5)(3)(8)$ [3]. It reduces both the statistical and systematical uncertainty by about one order of magnitude. For a g-factor determination from our measured frequency ratio the uncertainty of 4×10^{-10} in the electron mass dominates. Moreover, the uncertainty of the theory has not changed from our previous g-factor determination [3]. Therefore, our measurement cannot be considered as a more stringent test of the BS-QED calculation yet. However, the result presented here will allow for a better test when more precise calculations, as well as a more precise value for the electron mass, are available. This holds, in particular, for the $(Z\alpha)^6$ term of the two-loop QED correction, for which an upper limit of 1.7×10^{-9} is presently quoted [16]. Alternatively, our method can be used for a mass determination of isotopes. In our case of ^{28}Si the uncertainty of the ion mass of 2.5×10^{-11} is just below the statistical uncertainty. This is not the case when we apply our method, e.g., to ^{30}Si. Here, the mass uncertainty is 7.7×10^{-10} [17]. In addition, the nuclear recoil and structure contributions are small and sufficiently well calculated, which makes it possible to improve the accuracy of the mass of ^{30}Si significantly by comparing the electron g factors of $^{30}\mathrm{Si}^{13+}$ and $^{28}\mathrm{Si}^{13+}$. This holds in a similar way for other elements when the mass of one isotope is better known than that of a different one. Hydrogenlike $^{12}\mathrm{C}^{5+}$ represents a particular case since there is no uncertainty in the atomic mass and the binding energies of the electrons have been measured very accurately [15]. The BS-QED corrections are calculated to the 10^{-11} level [16]. Assuming a similar experimental precision as in the present case of $^{28}\mathrm{Si}^{13+}$, the remaining largest uncertainty in the g-factor evaluation arises from the electron mass. Thus, an adjustment of the electron mass to match experimental and theoretical results would lead to a mass value which is about an order of magnitude more accurate than the presently best-known value [13].

The authors acknowledge the contributions (especially Fig. 1) from J. Zatorski, Z. Harman, and C. H. Keitel. This work was supported by the Max-Planck Society, the Helmholtz Alliance HA216/EMMI, and the E.U. (ERC Grant No. 290870 - MEFUCO).

[1] H. Häffner, T. Beier, N. Hermanspahn, H.-J. Kluge, W. Quint, S. Stahl, J. Verdú, and G. Werth, Phys. Rev. Lett. **85**, 5308 (2000).

[2] J. Verdú, S. Djekić, H. Häffner, S. Stahl, T. Valenzuela, M. Vogel, G. Werth, H.-J. Kluge, and W. Quint, Phys. Rev. Lett. **92**, 093002 (2004).

[3] S. Sturm, A. Wagner, B. Schabinger, J. Zatorski, Z. Harman, W. Quint, G. Werth, C. H. Keitel, and K. Blaum, Phys. Rev. Lett. **107**, 023002 (2011).

[4] S. Sturm, A. Wagner, B. Schabinger, and K. Blaum, Phys. Rev. Lett. **107**, 143003 (2011).

[5] J. Zatorski, Z. Harman, and C. H. Keitel (private communication).

[6] B. Schabinger, S. Sturm, A. Wagner, and K. Blaum, Eur. Phys. J. D **66**, 71 (2012).

[7] L. S. Brown and G. Gabrielse, Phys. Rev. A **25**, 2423 (1982).

[8] R. S. Van Dyck, Jr., F. L. Moore, D. L. Farnham, and P. B. Schwinberg, Phys. Rev. A **40**, 6308 (1989).

[9] J. V. Porto, Phys. Rev. A **64**, 023403 (2001).

[10] J. D. Jackson, *Classical Electrodynamics* (Wiley & Sons, New York, 1975), 2nd ed.

[11] X. Xiang, P. B. Grosshans, and A. G. Marshall, Int. J. Mass Spectrom. Ion Processes **125**, 33 (1993).

[12] B. D'Urso, B. Odom, and G. Gabrielse, Phys. Rev. Lett. **90**, 043001 (2003).

[13] P. J. Mohr, B. N. Taylor, and D. B. Newell (2012), http://physics.nist.gov/constants.

[14] M. Redshaw, J. McDaniel, and E. G. Myers, Phys. Rev. Lett. **100**, 093002 (2008).

[15] W. Martin and R. Zalubas, J. Phys. Chem. Ref. Data **12**, 323 (1983).

[16] K. Pachucki, A. Czarnecki, U. D. Jentschura, and V. A. Yerokhin, Phys. Rev. A **72**, 022108 (2005).

[17] A. Wapstra, G. Audi, and C. Thibault, Nucl. Phys. A **729**, 129 (2003).